BIOMICROFLUIDICS **9**, 014111 (2015)

Colored polydimethylsiloxane micropillar arrays for high throughput measurements of forces applied by genetic model organisms

Siddharth M. Khare,[1] Anjali Awasthi,[2,3] V. Venkataraman,[1,a)] and Sandhya P. Koushika[4,a)]
[1]*Department of Physics, Indian Institute of Science, Bangalore 560012, India*
[2]*Department of Biological Sciences, BITS-Pilani, Pilani 333031, India*
[3]*NCBS-TIFR, Bangalore 560065, India*
[4]*DBS-TIFR, Homi Bhabha Road, Mumbai 400005, India*

(Received 23 October 2014; accepted 15 January 2015; published online 29 January 2015)

Measuring forces applied by multi-cellular organisms is valuable in investigating biomechanics of their locomotion. Several technologies have been developed to measure such forces, for example, strain gauges, micro-machined sensors, and calibrated cantilevers. We introduce an innovative combination of techniques as a high throughput screening tool to assess forces applied by multiple genetic model organisms. First, we fabricated colored Polydimethylsiloxane (PDMS) micropillars where the color enhances contrast making it easier to detect and track pillar displacement driven by the organism. Second, we developed a semi-automated graphical user interface to analyze the images for pillar displacement, thus reducing the analysis time for each animal to minutes. The addition of color reduced the Young's modulus of PDMS. Therefore, the dye-PDMS composite was characterized using Yeoh's hyperelastic model and the pillars were calibrated using a silicon based force sensor. We used our device to measure forces exerted by wild type and mutant *Caenorhabditis elegans* moving on an agarose surface. Wild type *C. elegans* exert an average force of $\sim$1 μN on an individual pillar and a total average force of $\sim$7.68 μN. We show that the middle of *C. elegans* exerts more force than its extremities. We find that *C. elegans* mutants with defective body wall muscles apply significantly lower force on individual pillars, while mutants defective in sensing externally applied mechanical forces still apply the same average force per pillar compared to wild type animals. Average forces applied per pillar are independent of the length, diameter, or cuticle stiffness of the animal. We also used the device to measure, for the first time, forces applied by *Drosophila melanogaster* larvae. Peristaltic waves occurred at 0.4 Hz applying an average force of $\sim$1.58 μN on a single pillar. Our colored microfluidic device along with its displacement tracking software allows us to measure forces applied by multiple model organisms that crawl or slither to travel through their environment. © *2015 AIP Publishing LLC*.
[http://dx.doi.org/10.1063/1.4906905]

I. INTRODUCTION

The physical environment of an organism can influence its locomotory behaviour through its ability to sense touch, in other words, through the physical forces that it experiences. Therefore, measuring forces applied or applying quantifiable forces on organisms can provide insights into both locomotory and mechanical responses for the organism as a whole. Such

a)Authors to whom correspondence should be addressed. Electronic addresses: venki@physics.iisc.ernet.in and spkoushika@tifr.res.in

information can be especially valuable if quick, reliable, and accurate measurements can be made using genetic model organisms that allow investigators to manipulate locomotion and other behaviours using genetic tools. Mechanical forces applied by organisms have typically been measured to understand the kinematics of locomotion. Techniques such as force plates, strain gauges, piezo-resistive sensors, micro-machined sensors, calibrated micropillars, and cantilevers have been employed with animals ranging in size from a few 100s of microns to a few centimeters.[1–7] Force measurements have also been carried out at lower length scales of 10s of microns for instance using individual cells. To investigate the role of the mechanical/physical environment, one can change the stiffness and/or viscosity of the surrounding medium or the substratum using biocompatible hydrogels.[8–12] Such hydrogel based devices are not reusable and calculation of forces applied can be challenging as the forces are distributed over a large surface.[13] Another means to measure the mechanical response of small multicellular organisms and cells is to use a micro-fabricated cantilever, for example, an atomic force microscope tip[14–17] or a micro-machined silicon cantilever.[18] These devices have high sensitivity and can be calibrated precisely for high accuracy. But this method enables measurements only at a single point at a given time and often not for a freely moving organism or cell. Attempts to overcome these limitations and make several parallel force measurements have resulted in two types of devices with (i) a micro-fabricated cantilever array[19] and (ii) SU8 polymer pillars mounted on SU8 cantilevers with metal strain gauges.[6] However, both devices are difficult to fabricate and the former measures forces only along a single axis where as a moving animal may apply force along multiple axes (x, y, and z).

Micropillar arrays made of elastic polymers like Polydimethylsiloxane (PDMS) provide a means to get reliable data using simpler fabrication steps that combine parallel force measurements along the entire organism and measurements along more than one axis. PDMS is a suitable polymer due to its biocompatibility,[20,21] chemical stability,[22] modifiable stiffness,[23–25] and ability to be reused. PDMS micropillars can measure forces in the range of pico-Newtons to 100s of micro-Newtons.[6,13,26–28] Typically, in a PDMS device, forces are measured by determining deflection using optical imaging under a microscope.[13] For example, Tan *et al.*[13] have used PDMS micro-needle arrays to measure forces in the range of few 10s of nano-Newton exerted by smooth muscle cells. In another study, the nematode worm *Caenorhabditis elegans* (*C. elegans*) has been shown to exert a few 10s of micro-Newton forces while moving in PDMS micropillar arrays.[7,28] Despite these advantages, a major limitation of such devices is poor image quality. Since PDMS is a translucent material there is often poor contrast between the objects studied and the pillars thus increasing the difficulty in tracking the object of interest reliably. This problem is especially acute when a liquid meniscus is present, which is typically the case with any biological sample. Thus, data analysis often requires time-consuming manual measurements or requires developing complex algorithms to automate this step.[7]

In our study, we address this issue and use our new device with two genetic models *C. elegans* and *Drosophila melanogaster* (*D. melanogaster*). We develop a method of fabricating colored PDMS devices. Coloring PDMS with ink and silicone pigments has been used to make optical filters[29] and to visualize small channels.[30] We have adapted a similar method to color just the micropillars selectively. Mechanical properties of colored PDMS as well as non-colored PDMS were characterized using uniaxial tensile testing. Because of batch to batch variations in the material properties of PDMS and possible lithographic fabrication errors, it is important to calibrate the micropillars directly.[27] We calibrated stiffness of the micropillars using a Femto Tools micro force sensor. We then implemented a finite element analysis (FEA) model for the micropillar using Comsol Multiphysics™ software package to obtain corrected values for the material parameters and the pillar stiffness. The colored pillars allowed us to use a simple 2D cross-correlation based algorithm to automate pillar identification and tracking. The semi-automated graphical user interface (GUI) built in Matlab™ simplified the process of data extraction from recorded images. We used our colored micropillar arrays and GUI to measure the force patterns of the nematode *C. elegans*. Utilizing our simple algorithm and the user interface, we were able to record data for 180 worms of 9 different mutant strains that include

strains defective in their body wall muscles and strains defective in detecting mechanical forces. We show that the body wall muscles of *C. elegans* are important in generating force during locomotion. To demonstrate the broad utility of our colored micropillars, we measured, for the first time, the forces exerted by *D. melanogaster* larvae during their locomotion. We show that the color of the pillars makes it possible to measure the deflection of the pillars that are otherwise difficult to detect. We were able to successfully record the peristaltic rhythm of the body wall muscles of *Drosophila* larva using colored micropillars.

II. EXPERIMENTAL METHODS

A. Material preparation

Orange G, rhodamine, and curcumin were tested to make colored PDMS. These dyes need to be dissolved in an organic solvent like methanol prior to mixing with PDMS. This process has two disadvantages: Methanol makes PDMS less viscous and the dyes are often highly soluble in the solvents used. The dye diffuses into the non-colored part of the device before PDMS is cross-linked thus increasing difficulty in selectively coloring a part of the device. (Refer to "Device Fabrication" for additional details.) The concentration of the dye required to visualize the color of the pillars through the microscope is large since in our case a large area ($\sim$3–4 mm^2) needs to be visualized. The dyes mentioned above are expensive when large amounts are needed. Therefore, we used the commercially available pigment AUS Orange (Asian Paints, India) to impart color to selective PDMS microstructures. PDMS (Sylgard 184) (10:1 base:curing agent ratio) was mixed with different dye concentrations, namely, 0%, 1%, 2%, 3%, 5%, 10%, 20%, and 30% by weight of PDMS. It is important to mix the dye thoroughly with PDMS to avoid non-uniformity. The mixture is then degassed in a vacuum desiccator for at least 10 min. Flat strips of approximately 1.5 mm thickness were prepared by pouring dye-PDMS composite on microscope slides. PDMS samples were also spin coated at 2000 rpm for 30 s on potassium bromide (KBr) pellets for Fourier Transform Infra Red (FTIR) spectroscopy. To ensure flatness, all the samples were cured on a levelled hotplate at 60 °C for 1 h before further curing in a convection oven at 100 °C for 18 h. FTIR samples were stored in a vacuum desiccator to avoid the moisture absorption by the KBr pellets.

B. Material characterization

We observed a large reduction in the stiffness of PDMS on addition of dye. Therefore, it was necessary to estimate the material parameters and mechanical properties of the dye-PDMS composite. Mechanical characterization of PDMS silicone using tensile testing has been demonstrated by several groups.[24,25,31–33] In our work, colored PDMS samples with a rectangular cross section were tested using Mecmesin MultiTest tensile testing machine (Figure 1(a)). Samples with 5 cm length and approximately 4 mm $\times$ 1.5 mm cross-section were fabricated for uniaxial tensile testing (schematic in Figure 1(b)). Three samples for each dye percentage were tested. Samples were stretched along the length at a quasi-static rate of 2 mm/min. This ensured that the force is measured at a steady state. Because PDMS is a nearly incompressible material (Poisson's ratio $\sim$ 0.5), the samples tend to slip from the clamps holding them. Therefore, to measure the actual stretch ratio, the central 2 cm region on the test specimen was marked using ink. The stretching experiment was video recorded and the stretch ratio was later determined using the change in position of the central ink marks. Material parameters were estimated by fitting the uniaxial tensile test data to the Yeoh model.[34] FTIR spectra of thin film samples coated on KBr pellets were recorded in transmission mode in the range of 400 cm^{-1} to 4000 cm^{-1} at 0.2 cm^{-1} resolution using a Perkin-Elmer IR spectrometer.

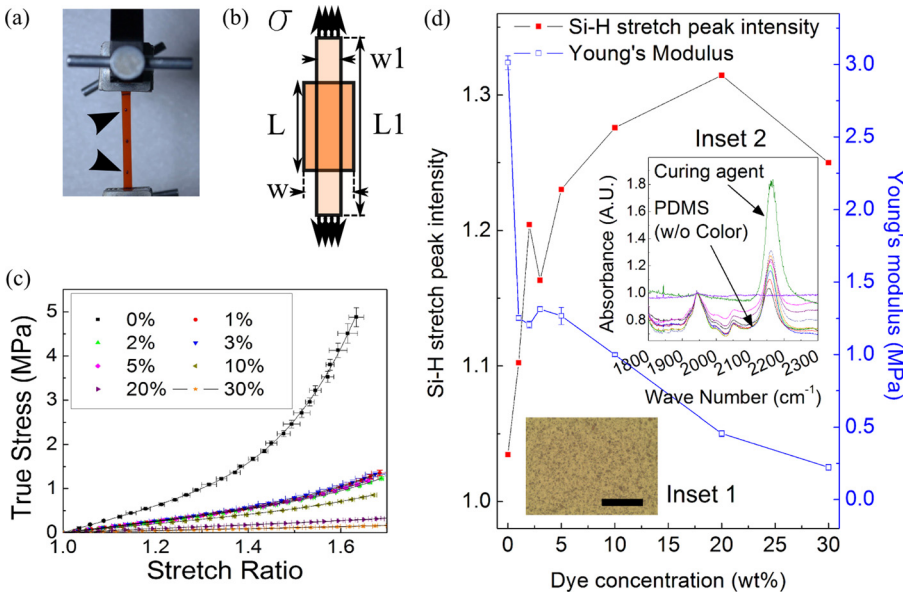

FIG. 1. (a) PDMS sample held in grippers for uniaxial tensile testing. The positions of the dots marked (indicated by arrow heads) in the central region of the sample were tracked to measure the stretch ratio. (b) Schematic of uniaxial stretching experiment. L and w are the initial length and width of the specimen and L1 and w1 are length and width after applying true stress σ along the length, respectively. (c) True stress versus stretch ratio for different dye-PDMS composite samples and the fit using Yeoh hyperelastic model (Eq. (3)). (d) Left axis: Si-H stretching mode absorption peak intensity, Right axis: Young's modulus at small deformations of dye-PDMS composite determined using Eq. (3) fit to uniaxial tensile test; as functions of weight concentration of dye. Error bars indicate $\pm$SD. (Inset 1): Microscopic image of 3% dye-PDMS composite thin film coated on glass cover slip (scale bar: 100 μm). (Inset 2): FTIR data of Si-H stretch absorption peaks at 2160 cm^{-1} of PDMS samples. Peak height increases as the dye concentration increases indicating an increase in the number of Si-H bonds and corresponding decrease in the crosslink density of PDMS.

C. Device fabrication

The device was designed to contain a bed of colored micropillars placed in a hexagonal array. Pillar diameter was 50 μm and the nearest neighbour edge to edge spacing was 70 μm. Non-colored PDMS micropillars of similar dimensions have been reported earlier.[7,28] Figure 2 provides the schematic of the process flow for colored PDMS micropillar array fabrication. We used soft lithography on SU8 to make the master mould. SU8 2100 was spun on a polished silicon wafer to obtain a film thickness of 150 μm. The coated wafer was then baked on a leveled hotplate at 95 °C for 45 min. UV exposure through a chrome mask was done using Oriel instruments UV light system. An SU8 master mould with micro-holes was obtained after developing. AUS Orange Dye (20% by weight) was mixed with PDMS base and curing agent mixture (10:1 ratio). The resulting colored PDMS was degassed in vacuum a desiccator to remove all trapped air bubbles and poured on the SU8 master mould. The master mould with the colored PDMS was degassed again in a vacuum desiccator at least for 10 min to remove all the air bubbles trapped in the micro-structures. The master mould was then removed from vacuum and the colored PDMS was wiped off with lint-free tissue paper. This was done gently such that colored PDMS filled in the microstructures in the master mould was not absorbed into the tissue paper. Fresh and non-colored PDMS (10:1 base to curing agent ratio) was then poured to a thickness of 1 mm on the master mould and cured on a leveled hot plate at 60 °C for 1 h and in a convection oven at 100 °C for 9 h. After curing, the device was allowed to cool to room temperature for at least half an hour before peeling it off from the master. The peeled PDMS device was further cured in the oven at 100 °C for 9 h to ensure complete cross-linking of PDMS. The Young's moduli of PDMS ranging from 1 MPa to ~3 MPa have been reported for various combinations of curing temperature and curing time.[23,31,35,36] Hence, the same temperature and curing times were used for bulk samples as well as micropillar devices. The micropillars were

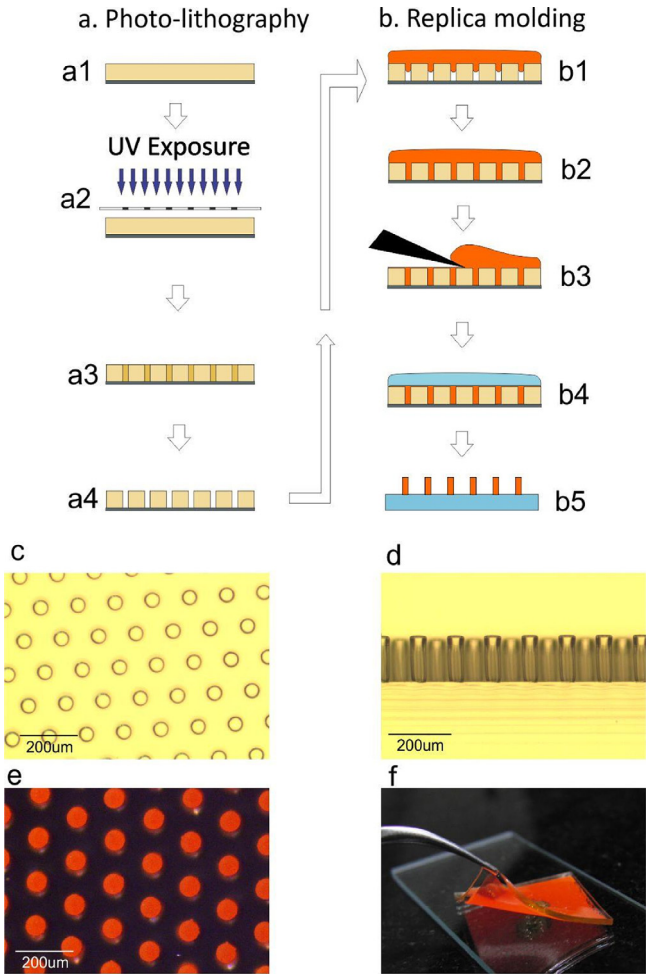

FIG. 2. (a1) SU8 spin coated on silicon wafer and softbaked (95 °C for 45 min on hotplate). (a2) Coated wafer exposed to UV light through a photo mask. (a3) Post exposure bake (65 °C for 1 min, 95 °C for 5 min on hotplate). (a4) SU8 developed in SU8 developer for 5–8 min to get master mould with holes. Silanize with Trichloro(1H,1H,2H,2H-perfluorooctyl) silane for 10 min in vacuum. (b1) AUS orange dye (20% by weight) and PDMS (Sylgard 184, 10:1 base to curing agent ratio) mixture poured on master mould, (b2) Degas in vacuum desiccator, (b3) Remove excess colored PDMS, (b4) pour clear PDMS (10:1) and cure at 60 °C on hotplate for 1 h and at 100 °C in a convection oven for 9 h, (b5) Peel off the cured PDMS device after cooling to room temperature and cure again at 100 °C in oven for 9 h to ensure complete cross-linking. (c) Top view of non-colored PDMS micropillars (d) Side view of non-colored PDMS micropillars. (e) Top view of colored PDMS micropillars. (f) Colored PDMS micropillar device on microscope slide.

calibrated using the FemtoTools force sensor. The FEA model of the pillar was implemented using Comsol Multiphysics™ software package.

D. Organism culture and imaging

1. C. elegans

Worms were cultured on NGM plates with *E. coli* OP50 as food source and at 22 °C temperature. Young adult animals were imaged which were obtained by picking L4 animals and imaged within 12–15 h time span. Wild type (N2),[37] a long strain *lon-2*(*e678*),[37] a dumpy strain *dpy-5*(*e61*),[37] muscle defective strains *unc-54*(*e675*)[38,39] and *unc-52*(*e669*),[40] and mechanosensory defective strains *mec-7*(*e1343*),[41] *mec-12*(*e1605*),[42] *mec-12*(*e1607*),[42] and *mec-4*(*e1339*)[42] were used. A thin pad of agarose (2% in distilled water) was prepared on a microscope slide. To ameliorate the possible dehydration of the worm and the attendant reduction in image quality, we placed this hexagonal pillar array on top of the agarose pad that contained worms in a

droplet of M9 buffer. The micropillar device was placed such that the pillar tips contact both the young adult worms and the agarose pad. Similar arrangements have been described in previous studies by Johari *et al.*[28] and Doll *et al.*[6] A schematic of our experimental setup is shown in Figure 3(a1). After ∼30 s during which the worm acclimatizes to the device, time lapse images of the worm movement in the chip were recorded at 15 frames per second (fps) with a 4× objective on an inverted compound microscope for 30 s using a color camera that was essential to capture the color of the micropillars (Figure 4, Multimedia view). The images were recorded within a total duration of 2 to 3 min. Instead of back illumination a light source was placed transversely to improve the contrast between the background and the pillars.

2. D. melanogaster

Canton-S (wild type) flies were raised in corn flour, D-glucose, agar containing propionic acid, methyl para-hydroxy orthophosphoric acid, and yeast (Bangalore fly media protocol) and were grown at 22 °C. The device was exposed to oxygen plasma using a Harrick plasma system at 38 W for 2 min to make the device hydrophilic before the experiment. The device was placed on a microscope slide with pillar tips facing upwards and a drop of PBS buffer was

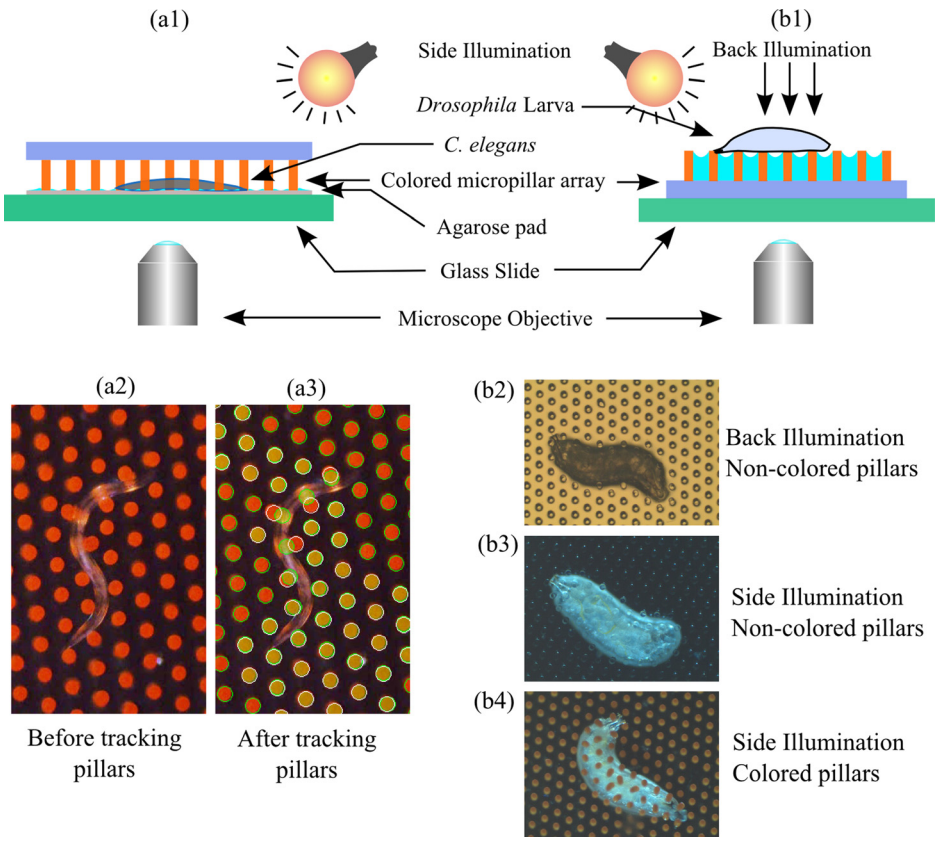

FIG. 3. (a1) Schematic of experimental arrangement for force measurement of *C. elegans* moving on agarose surface with a drop of M9 buffer. (a2) Image of worm in between colored PDMS micropillars. (a3) Same image as "a2" after tracking the pillar tip motion using matlab code, green overlay is applied to selected pillars. Green boundary indicates the reference position, while white boundary is the deflected position of pillar tip. (b1) Schematic of experimental setup for measurement of force exerted by *D. melanogaster* larva. (b2) Image of the larva recorded using non-colored PDMS micropillars and back illumination. (b3) Image of the larva recorded using non-colored PDMS micropillars and side illumination. (b4) Image of the larva recorded using colored PDMS micropillars and side illumination. Pillars are clearly visible only with the colored device. Figures 3(b1), 3(b2), 3(b3), and 3(b4) reprinted with permission from Khare *et al.*, 18th International conference on Miniaturized Systems for Chemistry and Life Sciences, 2014. Copyright 2014 The Chemical and Biological Microsystems Society.

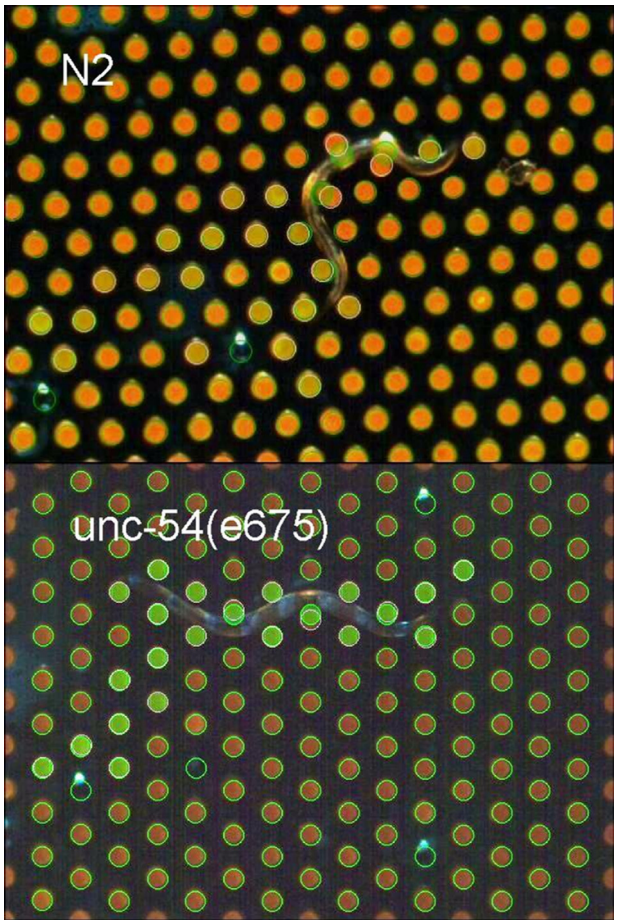

FIG. 4. Movies of a wild type (N2) and muscle mutant (*unc-54*(*e675*)) young adult *C. elegans* moving on agarose surface in between the colored PDMS micropillars. The movies were recorded using 4× objective on an inverted compound microscope using a color camera. Frame rate of 15 fps was used. Sample was illuminated transversely with a light source at an angle instead of a standard back illumination to improve contrast. Refer to Figure 3(a1) for detailed experimental schematic. Selective pillars in the movie have been tracked. Green circles around the pillars indicate the reference positions of all the pillars in the image. Green overlay indicates that the pillar is selected for deflection tracking. White circles are the deflected positions of the pillar tips. (Multimedia view) [URL: http://dx.doi.org/10.1063/1.4906905.1]

added to fill the gaps between the micropillars. A first instar larva was transferred to the pillars using a brush. Imaging was carried out using an inverted compound microscope with a 4× objective positioned below the pillar device and images recorded at 15 fps on a color camera (schematic in Figure 3(b1), Multimedia view of Figure 5).[43]

E. Automation of pillar tracking

In the applications where the pillar deflections need to be tracked dynamically and at multiple points in large number of images, automation can significantly reduce the time required for data analysis. Therefore, we developed a semi-automated graphical user interface (GUI) using Matlab™ to facilitate pillar tracking with minimal user intervention. The colored micropillar device improves contrast compared with the previously demonstrated non-colored devices.[7,28] Typically, since organisms studied using such devices are translucent, complex algorithms are necessary to separately identify the pillar and the organism. The color of the pillar allowed us to develop a simple algorithm to identify and track the pillar (Figure 6(a)). A template image consisting of a white circle of diameter equal to the pillar diameter in pixel units was generated. A 2 dimensional (2D) cross-correlation between the thresholded microscopic image and the template image was calculated. The position of the template where the cross-correlation reaches a maximum is

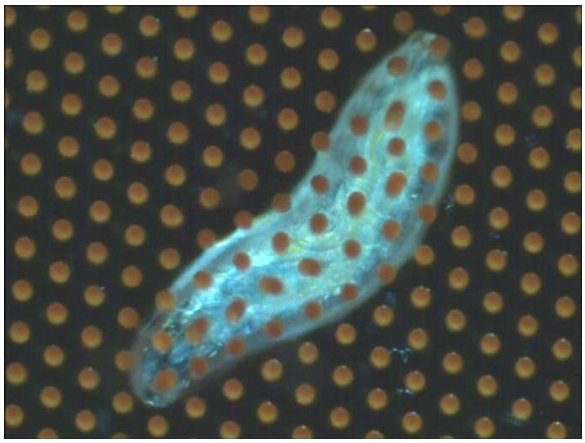

FIG. 5. Movie of a first instar *D. Melanogaster* (*Canton-S*) larva moving on the colored PDMS micropillars tips. The movie is recorded using 4× objective on an inverted compound microscope using a color camera. Frame rate of 15 fps was used. Sample was illuminated transversely with a light source at an angle instead of a standard back illumination to improve contrast. Refer to Figure 3(b1) for detailed experimental schematic. (Multimedia view) [URL: http://dx.doi.org/10.1063/1.4906905.2]

recorded as the pillar position in the image. Figures 6(b), 6(c), 6(d), and 6(e) show images of a pillar touching the body of a *C. elegans*, the template image, the thresholded image, and the 2D cross correlation between the template and the thresholded image, respectively. Figures 3(a2) and 3(a3) show the pillar images before and after tracking using the algorithm described.

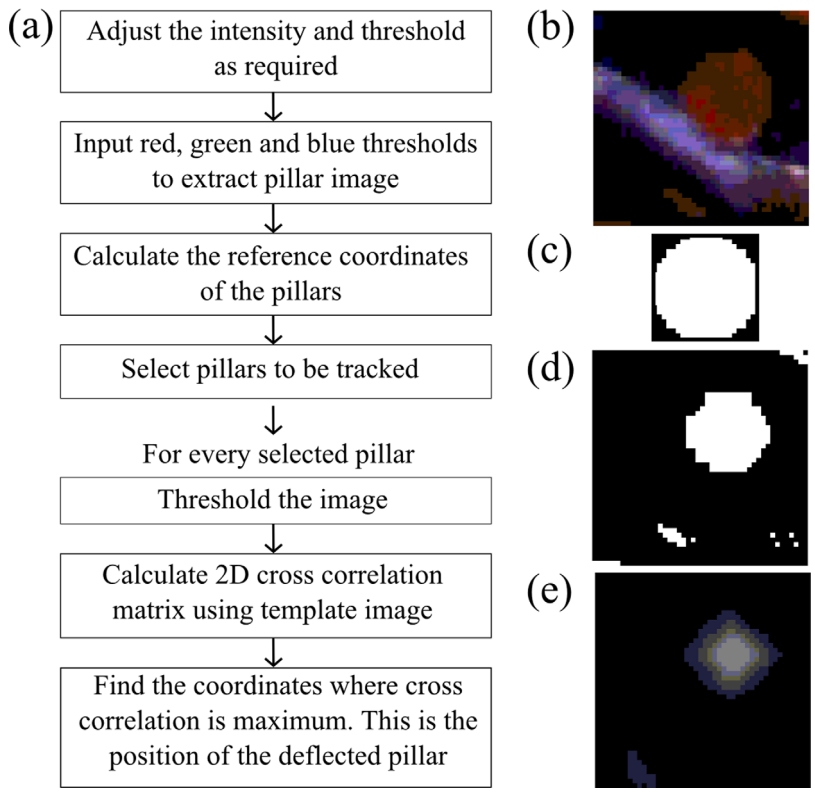

FIG. 6. (a) Algorithm used for tracking pillar tip motion. (b) Image showing colored pillar touching body of worm *C. elegans*. (c) Template image used for cross-correlation. (d) Colored pillar image extracted after thresholding red, green, and blue channels. (e) 2D cross correlation matrix of template and the thresholded image showing a maximum value (indicated as a lighter shade) at the center of the pillar.

The graphical interface allows the user to (i) adjust the brightness and contrast of the images, (ii) select the length of the movie to be analyzed, and (iii) set the frame rate at which the analysis is desired. The threshold levels for red, green, and blue channels should be set before tracking such that only the parts of the image with pillars are thresholded. After selecting any two pillars in a row that are not deflected and specifying the number of pillars in between them, the program automatically calculates the reference (non-deflected) positions of the pillars. Then the pillars that are to be tracked are selected using the mouse. After this point, there is no necessity for human intervention until all pillars are tracked. (See Ref. 80 for screenshots of GUI in supplementary Figure 1.) Tracking one image frame with about 30 pillars takes ∼75 ms when the GUI is used. In comparison, manual tracking of such a single image takes several minutes.

F. Parameters calculated

We analyzed 8 s of movie (120 frames at 15 fps) for every *C. elegans*. The 8 s duration was selected such that the worm remained in the field of view of the microscope and there was no motion of the microscope stage. These 8 s can lie anywhere in the recorded 30 s. *Drosophila* movies were analyzed by excluding the frames that did not show the entire larval body and those that showed microscope stage motion. Following parameters were analyzed:

(1) **Body length**: Length of *C. elegans* from anterior end to posterior end (i.e., head to tail) measured manually from the recorded image. The "segmented line" tool from the software package ImageJ (Ref. 44) was used to draw and measure the length of a segmented line curved along the central longest axis of the worm.
(2) **Body diameter**: The width of the thickest region of *C. elegans* was measured manually from the recorded image using ImageJ. This width is called the body diameter in this paper.
(3) **Total average force per animal**: Sum of forces exerted by the animal on all the pillars touching its body in every frame was calculated and averaged over all the frames in the movies for *C. elegans*. Only the pillars that are deflected by more than 2 pixels were considered deflected. In case of *Drosophila*, deflected pillars were imaged as projections of the full lengths of the pillars (Figure 3(b1)). Thus, an ellipse was fitted on every pillar using "Analyze particles" tool in ImageJ to obtain the major axis lengths of the fitted ellipses. The diameter of the pillar was then subtracted from the major axis lengths to obtain the deflection and consequently the force exerted on every pillar.
(4) **Average force applied per pillar (*Fpp*)**: This is calculated as the total average force divided by an approximate number of pillars that a worm body touches in every single movie frame and then averaged over all the frames. The smallest distance between the pillar centers in our micropillar array is 120 μm. Therefore, the micropillar array consists of approximately 1000 μm/120 μm = 8.33 pillars per millimeter of the device. Thus, the approximate number of pillars that a given *C. elegans* can touch at a time is calculated as (body length in millimeters) × 8.33 (see Ref. 80 for supplementary Table I).
(5) **Maximum force on a single pillar**: Maximum force applied on a single pillar that is deflected the most by an animal in the entire movie, averaged over the number of animals analyzed.
(6) **Number of pillars touched by a worm (*Np*)**: Total number of pillars that a *C. elegans* touched in the full span of the movie was counted. This includes pillars that are not deflected. This is different from the number of pillars a worm touches in a single movie frame. The animals that move into a region with a pillar missing were excluded.

III. RESULTS AND DISCUSSION

A. Material properties

Colored and non-colored PDMS samples were characterised to determine the material parameters used to generate the FEA model of the micropillars. Since PDMS is a nearly incompressible rubber like material, we used the Yeoh model[34] to fit the uniaxial tension data. This

model has previously been used for modeling of rubber and soft tissues.[34,45–48] The model describes the strain energy density as a function of only the first invariant of the left Cauchy-Green deformation tensor, I_1,

$$W = c_1(I_1 - 3) + c_2(I_1 - 3)^2 + c_3(I_1 - 3)^3, \tag{1}$$

where c_1, c_2, and c_3 are the material parameters

$$I_1 = \lambda_1^2 + \lambda_2^2 + \lambda_3^2, \tag{2}$$

λ_i with $i = 1, 2, 3$ are the principal stretch ratios, which are the ratios of deformed lengths to the original lengths in the respective principal directions. For an incompressible material, $\lambda_1 \cdot \lambda_2 \cdot \lambda_3 = 1$ and in uniaxial tension, $\lambda_2 = \lambda_3 = 1/\sqrt{\lambda}$ and $\lambda_1 = \lambda$. For a perfectly incompressible material in uniaxial tension along the principal direction, the true stress in that direction is given as follows:

$$\sigma_1 = 2\left(\lambda^2 - \frac{1}{\lambda}\right)\left[c_1 + 2c_2\left(\lambda^2 + \frac{2}{\lambda} - 3\right) + 3c_3\left(\lambda^2 + \frac{2}{\lambda} - 3\right)^2\right]. \tag{3}$$

This relation has been used to find the material constants c_1, c_2, and c_3 from experimental data. True stress was determined using the equation, $\sigma_1 = F\lambda/A_0$, where A_0 is the initial cross sectional area and F is the force measured in uniaxial test. The true stress-stretch data were used to fit the hyperelastic material model defined by Eq. (3) using Levenberg-Marquardt nonlinear curve fitting algorithm using Origin™ software package. The shear modulus for a Yeoh form material at small deformations is given by $\mu = 2c_1$ (see Ref. 80 for supplementary material for the derivation) which was used to determine the Young's modulus of the PDMS samples. Figure 1(c) shows the Yeoh model fit to the experimental data for PDMS samples with different dye concentrations. The Young's modulus for small deformations varied from 3.01 ± 0.05 MPa to 0.22 ± 0.02 MPa when dye concentration in the PDMS was increased from 0% to 30% (Figure 1(d) right Y-axis).

We performed FTIR analysis of the dye-PDMS composite samples to account for the observed change in Young's modulus for small deformations. Inset 1 in Figure 1(d) shows a microscopic image of dye-PDMS composite wherein the dye particles appear to act like a filler in the PDMS matrix. Filler materials, such as carbon black, silica, and carbon nano-tubes, have been shown to increase the elastic modulus of the PDMS composites.[49–52] On the contrary, in the case of AUS Orange dye we observed that the Young's modulus decreases from 3.01 ± 0.05 MPa for pure PDMS to 0.22 ± 0.02 MPa for the 30% dye-PDMS composite (Figure 1(d)). We propose that the change in crosslink density can cause the observed reduction in the Young's modulus. The intensity of the absorption peak around 2160 cm^{-1} was observed to increase as the dye percentage in PDMS was increased (Figure 1(d)). It rises to a maximum value of 1.81 for pure curing agent (Figure 1(d)—inset 2). This peak corresponds to the Si-H stretching mode.[53] The inset 2 in Figure 1(d) shows the FTIR absorption spectra normalized with respect to the absorption peak at 1944 cm^{-1}. In the process of curing, the Si-H groups in the curing agent react with the PDMS base.[54] The intensity of Si-H stretch peak is proportional to the number of Si-H groups in the sample. Thus, higher the peak intensity, lower is the crosslink density. These observations support the conjecture that the dye affects the crosslinking of PDMS.

B. Micropillar calibration

Calibration of the micropillar stiffness is essential to convert the measurements of pillar tip deflections to forces. The micropillars were imaged under the optical microscope (Figures 2(c)–2(e)) and the following measurements were made: mean pillar height 153 μm (SD = 5.24 μm, n = 40), mean pillar diameter 50 μm (SD = 0.58 μm, n = 152), and edge to

edge pillar spacing 70 μm (SD = 0.58 μm, n = 152). Colored PDMS pillars (dye concentration 20% by weight of PDMS) were calibrated using the FemtoTools force sensor (Figure 7(a)). The sensor touched the pillar approximately 25 μm–30 μm away from the tip. The pillar was pushed by the sensor and the deflection at the point of contact was measured optically under a microscope. The FemtoTools force sensor that is made out of single crystal silicon generates an output voltage proportional to the force applied on the tip of a silicon cantilever. This voltage was measured to obtain force-deflection curves for the colored micropillars (Figure 7(b) scatter plot).

A finite element model of the pillar was generated using the Comsol Multiphysics^{TM} software package. The actual shapes of five pillars were traced from the microscopic images to reproduce the pillar geometry as accurately as possible (Figure 7(b), inset). The Yeoh model was implemented to generate the force v/s tip deflection curves for the modeled pillars. Surprisingly, the values of the Yeoh parameter c_1 determined by uniaxial tensile testing of bulk PDMS samples did not reproduce the force-deflection data recorded using the FemtoTools sensor for the micropillars. The measured stiffness was 20% higher than the stiffness calculated by the FEA model that utilized the bulk c_1 value. Therefore, the value of the parameter c_1 was adjusted for every pillar to obtain an average of 0.094 ± 0.013 MPa (Figure 7(b), solid lines). This suggests that the material parameters measured for the bulk samples may not remain the same for the devices fabricated at a micro-scale despite using the same curing conditions for PDMS. These observations emphasize the necessity of calibrating the micropillars directly using a force sensor.

Although the FEA model reveals the nonlinear nature of the deflections, the force-deflection curve obtained using the FemtoTools sensor remains largely linear until deflections reach 60 μm. Thus, considering the errors in force measurement and the lithographic errors in

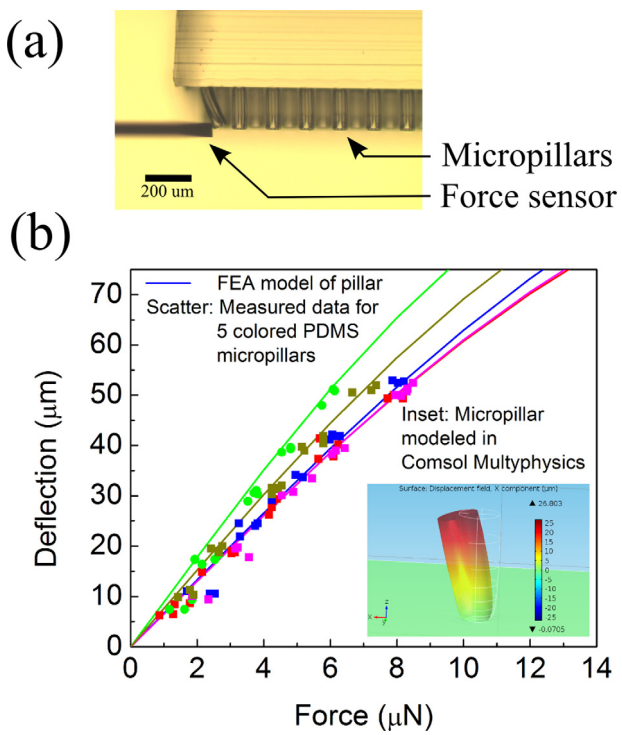

FIG. 7. (a) Microscopic photograph of force-deflection measurement of PDMS micropillar using FemtoTools force sensor. (b) The pillar deflections as a function of the force applied to the 20% dye-PDMS composite micropillars. Scatter symbols represent experimental data for the colored pillars measured using FemtoTools force sensor. Solid lines are the FEA simulations in Comsol Multiphysics^{TM} software with the value of material parameter c_1 adjusted to match the measured force-deflection data (scatter plot). The inset shows a rendered image of micropillar modeled in Comsol^{TM}. The color bar indicates the displacement in x direction from 0 μm (green) to 25 μm (red).

the pillar height and diameter, linear regression on the force-deflection curves from the FEA model gives a reasonable estimate of the pillar stiffness in 0 μN–8 μN force range. The stiffness of a micropillar can then be calculated using the linear relationship, $F = k^*x$. Here, F is the applied force, k is the average stiffness of the pillars, and x is the tip deflection. *C. elegans* touch the pillar approximately 25 μm away from the tip of the pillar, whereas the images recorded using the microscope while the *C. elegans* push against the pillars show the deflections of the pillar tips.[7] Therefore, the effective average stiffness of the micropillars was calculated in the FEA model of the pillar. The effective average stiffness of the 20% dye-PDMS micropillars was calculated to be 0.12 ± 0.01 μN/μm for *C. elegans* force measurements.

Pillar stiffness was calculated separately to measure forces applied by *Drosophila* larvae. *Drosophila* larvae touch the tips of the micropillars. Thus, the FEA model of the pillar with mean height of 153 ± 5.24 μm was used to obtain average pillar stiffness of 0.1 ± 0.01 μN/μm.

A different range of forces may be measured by changing the pillar dimensions. For example, approximate pillar stiffness of 0.02 μN/μm can be obtained with the pillar diameter set to 50 μm and the pillar length to 300 μm. Such pillars would detect forces from 0.2 μN to 1.4 μN in our system. The knowledge of material parameters will also be useful when a different Young's modulus is desired. Pillars with an altered Young's modulus can be used to alter the stiffness of the micropillars and thereby modify the force ranges that can be measured. Our device is reusable after cleaning using standard solvents such as like water and ethanol.

C. *C. elegans* force measurement

We used the colored micropillar device described above to measure the forces exerted by the worm *C. elegans* moving on an agarose surface with buffer to maintain animal health. Strains were chosen (i) to test the effect of body length along the anterior-posterior axis and diameter along the left-right axis on forces exerted by the animals, (ii) to test the effect of body wall muscles on forces exerted by *C. elegans*, and (iii) to test whether animals insensitive to gentle mechanical stimuli apply the same force on pillars as wild type animals. The genotypes/*C. elegans* strains we used for our analysis include wild type (N2), a long strain *lon-2*(*e678*), a dumpy strain *dpy-5*(*e61*), body wall muscle defective strains *unc-54*(*e675*) and *unc-52*(*e669*), and mechanosensation defective strains *mec-7*(*e1343*), *mec-12*(*e1605*), *mec-12*(*e1607*), and *mec-4*(*e1339*). Dumpy are shorter and fatter, while long animals are longer and thinner than wild type animals. *dpy-5* encodes a group I procollagen which is required for wild type body length and cuticle structure.[55] *lon-2* encodes a member of the glypican family of heparan sulfate proteoglycans that is required for negative regulation of a pathway that regulates body length.[56] *dpy-5*(*e61*) and *lon-2*(*e678*) animals have been reported to be softer (lower cuticle stiffness) than wild type due to changes in their cuticle proteins.[4,57] The altered cuticle stiffness could change the magnitude of the forces applied by the organism. The gene *unc-54* encodes the protein myosin heavy chain and *unc-52* encodes perlecan.[58,59] In *unc-54*(*e675*) animals, the body wall muscle structure is disrupted due to changes in the myosin heavy chain[38,39] and in *unc-52*(*e669*) animals, the myofilament assembly in body wall muscles is defective.[40,59] All mechanosensation defective strains tested alter the function of the six touch sensitive neurons known to mediate gentle touch in *C. elegans*. *mec-4* encodes a subunit of the mechanically gated channel expressed in these neurons, while *mec-7* and *mec-12* encode tubulin subunits known to be important in transducing the mechanical signal in these neurons.[60,61]

We observed that just after placing the pillar device on a worm, animals move very rapidly for about 30 s after which they resume regular locomotion. The initial rapid locomotion perhaps akin to avoidance behaviours that could arise from the sudden intense mechanical stimulation when the pillar device is first placed on the worm. Our video recordings start after this initial 30 s period. We analyzed 120 frames per worm (8 s movie at 15 fps) and on average 29 pillars were tracked per frame to generate approximately 600 000 data points. Tracking each pillar took ~2.5 ms per frame and therefore the tracking system can be expanded to real time imaging. The total average force enabled us to assign a single numerical value to every worm that represents the average force applied by the organism over the imaging time. Table I gives the

TABLE I. Total average force calculated for the *C. elegans* strains.

C. elegans strain (n ≥ 20 animals)	Total average force (μN)	Standard error of Mean (SEM) (μN)	Average force applied per pillar (*Fpp*) (μN)	Standard error of mean (SEM) (μN)	*p*-value with respect to N2
N2	7.68	0.76	1.00	0.17	1
lon-2(*e678*)	9.97	0.94	1.09	0.21	1
dpy-5(*e61*)	4.36	0.48	0.96	0.20	1
unc-54(*e675*)	3.49	0.33	0.48	0.08	0.013
unc-52(*e669*)	5.33	0.56	0.78	0.16	1
mec-7(*e1343*)	9.66	0.80	1.33	0.21	0.77
mec-12(*e1605*)	8.29	0.82	0.99	0.17	1
mec-12(*e1607*)	6.81	0.78	0.99	0.21	1
mec-4(*e1339*)	7.31	1.07	0.91	0.25	1

total average force values calculated for each *C. elegans* strain tested. The wild type (N2) animals exert a total average force (averaged over 120 frames) of about $7.68 \pm 0.76\,\mu$N in our device (Table I). The forces applied by wild *type C. elegans* in our pillar chip are similar to values reported earlier[28] (Table II). The average values of forces applied by wild type animals moving in the similar pillar array (50 μm spacing) lacking dye that were manually tracked also gave us similar values of $7.05 \pm 1.24\,\mu$N (n = 9). The differences in the values between animals of the same genotype and between genotypes occur because of the inherent variations in the body lengths of the animals and consequently the number of deflected pillars. The variations in body lengths among the animals of same strain range from 12% for *lon-2*(*e678*) strain to 23% for *mec-12*(*e1607*) strain. Therefore, we calculated the average force applied per pillar (*Fpp*) to mitigate the effect of inherent worm body length variations between strains (Figure 8(a1), Table I). *Fpp* for wild type young adult *C. elegans* was approximately $1.00 \pm 0.17\,\mu$N (Table I).

lon-2(*e678*) mutants have the highest mean body length and lowest diameter but it does not show any significant difference in *Fpp* compared to *dpy-5*(*e61*) which had the lowest body length and largest body diameter comparable to wild type (Figure 8(a1)). Johari *et al.* have shown that the force applied by the worm increases when the pillar spacing is reduced from 80 μm to 50 μm where they used worms with ∼80 μm body diameter. In our device, pillar spacing is maintained at 70 μm. This is always larger than the mean worm diameter for all the mutant strains. Thus, the effect of pillar spacing reported earlier was not observed in our

TABLE II. Comparison with previous reports on force measurements of *C. elegans*.

Doll *et al.*[6]	SU-8 force sensing pillars. Isolated force measurement pillars	Wild type Worm moves on agar	Forces exerted on single pillars $<10\,\mu$N
Ghanbari *et al.*[7]	PDMS micropillar array. Smallest inter-pillar spacing of 80 μm	Wild type Worm moves on PDMS	Forces exerted on single pillars Maximum force of 32.61 μN for 80 μm pillar spacing
Johari *et al.*[28]	PDMS micropillars array Inter-pillar spacing of 50 μm and 80 μm	Wild type Worm moves on PDMS	Forces generated by whole body Average force ∼20 μN for 50 μm pillar spacing and ∼8 μN for 80 μm pillar spacing
This study	Colored PDMS micropillars. Inter-pillar spacing 70 μm	Wild type and several mutant strains Worm moves on agarose	Forces generated by whole body Average Wild type force ∼7.68 μN

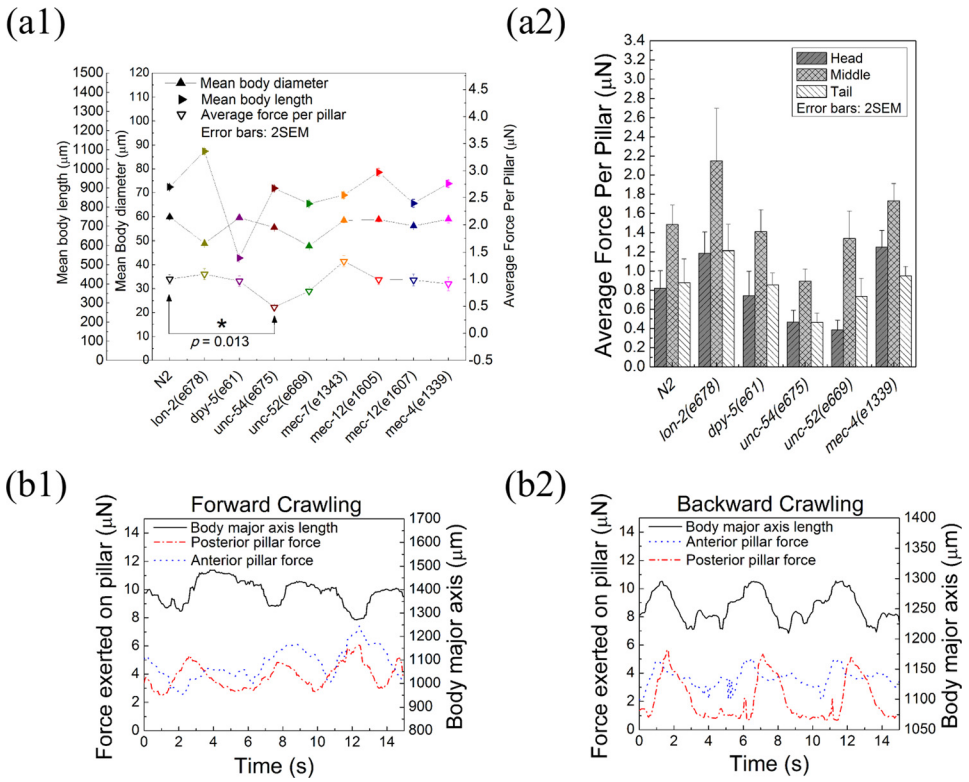

FIG. 8. (a1) Left Y axis 1: mean body length, Left Y axis 2: mean body diameter, right Y axis: Average force applied per pillar for different strains. Error bars are ±SEM (n ≥ 20 animals per strain). (a2) Average forces per pillar exerted by different body parts, namely, head, middle, and tail of the worm. Forces were measured for 5 worms of selected strains for 5 image frames each. Error bars are SEM for 5 animals per strain. (b1) and (b2) Dotted and dashed lines represent forces on the two selected pillars (anterior and posterior, respectively) near the centerline of *D. melanogaster* larva (left Y axis). Solid line represents the peristaltic contractions of the body wall muscles recorded as the major axis length of the body (right Y axis). (b1) shows forward crawling and (b2) shows reverse crawling. Figures 8(b1) and 8(b2) reprinted with permission from Khare *et al.*, 18th International conference on Miniaturized Systems for Chemistry and Life Sciences, 2014. Copyright 2014 The Chemical and Biological Microsystems Society.

experiments even when there were substantial differences in mean body diameters, approximately 18%, between *dpy-5*(*e61*) and *lon-2*(*e678*) mutants (Figure 8(a1)). The *Fpp* values did not vary when the inter-pillar distance changed from 100% to 140% of the body diameter. The average wild type force measured in our device (7.68 ± 0.76 μN, Table I) is similar to that reported by Johari *et al.* (∼8 μN) where the pillars were spaced 80 μm apart. Further, *dpy-5*(*e61*) worms despite having a significantly lower cuticle stiffness compared to wild type (N2) and *lon-2*(*e678*) worms (*dpy-5*(*e61*) 0.39 N/m, *lon-2*(*e678*) 0.67 N/m, N2 0.75 N/m),[4,57] did not show significant difference in *Fpp*. When external force is applied to the *C. elegans* body, *dpy-5*(*e61*) worms have been shown to be more sensitive to mechanical touch to the cuticle compared to the *lon-2*(*e678*) and wild type animals.[57] The same study demonstrated that the overall body stiffness correlates with the half maximal response probability independently for both force and indentation of the cuticle when a pre-defined force was applied to the worm body.[57] However, dynamic forces exerted by the worm on its environment while moving in its normal sinusoidal motion were not measured.

It has been reported that the body wall muscle contraction and relaxation governs the stiffness of the worm body[62] and consequently also modulates the sensitivity of the worm to sense external mechanical stimuli.[57] Thus, it is important to quantify the effect of the body wall muscles as well as the sensitivity of the worm to external mechanical stimuli on the forces generated during locomotion. The *Fpp* values for mutants *unc-54*(*e675*) and *unc-52*(*e669*) that have defective body wall musculature were approximately 0.48 ± 0.08 μN and 0.78 ± 0.16 μN,

respectively. These are smaller compared to wild type ($1.00 \pm 0.17\,\mu$N) (Figure 8(a1)). The *Fpp* value for *unc-54*(*e675*) is significantly lower compared to the wild type (N2) (p-value $= 0.013$, Table I). Our data suggest that the body wall muscles contribute significantly to the ability of *C. elegans* to apply force in a micro-structured environment. Further, to test the effect of defective mechanosensation on the forces generated, we measured the average force exerted by *C. elegans* with defects in mechanosensation where the neuron that senses touch was defective in various aspects of the touch sensory or transduction apparatus.[60,61] These mutant animals, namely, *mec-7*(*e1343*), *mec-12*(*e1605* and *e1607*), and *mec-4*(*e1339*), do not show a significant change in *Fpp* compared to wild type animals (Figure 8(a1)).

We also observed that different mutant strains showed different degrees of active locomotion in the device. This was quantified as the total number of pillars touched by the worm at least once while moving in the micropillar device for 8 s (*Np*). This number of pillars is proportional to the area of the device in which the worm traveled and thus represents the motility of the worm in the device (see Ref. 80 for supplementary Table I). It was observed that *Np* was largest ($\sim$26) for the wild type worms and smallest ($\sim$12) for the body wall muscle defective mutants whose body lengths were similar to the wild type (Figure 8(a1), Ref. 80 supplementary Table I). Moreover, mechanosensation defective mutants touched slightly fewer pillars ($Np \sim 16$–20) compared to wild type indicating slightly less motility than the wild type. The mutants with softer cuticle, *lon-2*(*e678*) and *dpy-5*(*e61*) also displayed reduced locomotion compared to wild type in the micropillar device (Ref. 80 supplementary Table I). Park *et al.*[63] have demonstrated that the mechanosensation defective and abnormal waveform mutants swim slower compared to the wild type on a structured agar plate and thus span a smaller area compared to wild type. Our experiments show similar results where crawling motion of worms is studied as opposed to swimming. Taken together our experiments show that forces applied by the worm on pillars during locomotion depends on its body wall muscles but not on the ability of the worm to sense externally applied force.

We also measured forces applied by different regions of the worm to determine if there might be region specific differences in force application that depend on the animal's ability to sense force. We examined 5 worms for each of the following genotypes N2, *lon-2*(*e678*), *dpy-5*(*e61*), *unc-54*(*e675*) and *unc-52*(*e669*), and *mec-4*(*e1339*). We selected 5 images from the recorded movies and divided the worm body into three sections, namely, head, tail, and middle. Nose to pharynx was called the head, the same length as the head region from the posterior end was designated as the tail, and the remaining central section was considered as the middle. The number of pillars touching a specific body part depends on the length of the worm. In case of wild type and mutants defective in mechanosensation, we observed that the head and the tail sections exerted comparable average force per pillar, whereas the middle of the worm exerted approximately 75% larger force per pillar compared to the extremities (Figure 8(a2)). The mutants defective in body wall muscles displayed smaller forces in all the three body parts compared to wild type. However, it is important to note that the central region still showed significantly larger force per pillar (91% for *unc-54*(*e675*) and 163% for *unc-52*(*e669*)) than the head or the tail while both of these were comparable to each other (Figure 8(a2)). Supplementary Figures 2 and 3 (Ref. 80) show the distribution of forces exerted on single pillars by the *C. elegans* strains N2, *lon-2*(*e678*), *dpy-5*(*e61*), *unc-54*(*e675*), *unc-52*(*e669*), and *mec-4*(*e1339*) where greater exerted force can be observed on the pillars touching the middle compared to those touching the head or the tail. The maximum forces exerted on a single pillar by N2, *lon-2*(*e678*), *dpy-5*(*e61*), *unc-54*(*e675*), *unc-52*(*e669*), and *mec-4*(*e1339*) animals were $3.76 \pm 0.63\,\mu$N, $3.56 \pm 1.41\,\mu$N, $2.59 \pm 0.73\,\mu$N, $2.06 \pm 0.06\,\mu$N, $2.44 \pm 0.74\,\mu$N, and $3.75 \pm 1.11\,\mu$N, respectively (averaged over 5 animals of each strain, $\pm$SD) (see Ref. 80 for supplementary Figures 2 and 3). The maximum forces of about $30\,\mu$N have been reported for wild type *C. elegans* that moved in a PDMS pillar arrays that lacked agarose[7,28] (Table II). Our data suggest that the presence of agarose as the substratum for worm locomotion affects the forces exerted by the worm on the micropillars.

The similar forces exerted by different mechanosensation defective *C. elegans* strains may depend in part on the differences in response to harsh touch compared to gentle touch. The

ability to sense touch in *C. elegans* is mediated by six touch receptor neurons: two ALMs, AVM, two PLMs, and PVM which span the body length; the ASH neuron that projects to the nose and the PVD and FLPs that envelope the body.[64] It has been demonstrated that transferring a worm from one plate to another using standard tools like a worm pick has long lasting effects on crawling locomotion parameters such as average speed, pausing during movement, and angle of body bends.[65] Such changes persist for 4–8 min (Ref. 65) and are thought to be largely mediated through the stimulation of the PVD neuron. In the absence of harsh forces that stimulate the PVD for instance when *C. elegans* swim in solutions with variable viscosities, the gentle touch neurons of ALM and PLM are shown to be important.[66] These prior studies suggest that placing a worm in our device using a platinum pick likely stimulates the PVD neuron. We recorded animal locomotion for a 30 s period within 2–3 min of the transfer of the worm to the device. In this time period, harsh stimulation through PVD may make a greater contribution to worm locomotion than the gentle touch neurons. To uncover the role of the gentle touch neurons, we may need to record locomotion 10 min after the animal is placed in our device. However, typically during this time the animal crawls out of the device limiting our ability to carry out the experiment.

The average force per pillar exerted by a young adult *C. elegans* is independent of its body length and its diameter (Figure 8(a1)). The central region of the worm generates much larger forces compared to the head or the tail of *C. elegans* (Figure 8(a2)). We show that the body wall muscles contribute to the ability of *C. elegans* to exert force on its environment during locomotion. Our data suggest that the overall ability to apply force may not depend either on cuticle stiffness or on the ability of the touch neuron to sense externally applied force at least within a span of several minutes after transferring the animal to the micropillar device. No changes in musculature have been reported in the mechanosensory defective *C. elegans* strains we tested and thus they may all be able to generate forces similar to wild type during locomotion. The motility of the *C. elegans* in the micropillar array was reduced slightly in the animals defective in mechanosensation and defective in their cuticle proteins. The motility was significantly reduced in *C. elegans* with defective body wall musculature. However, reduced motility does not necessarily reflect a reduced ability of the animal to generate forces for locomotion in between the micropillars (Figure 8(a1), Ref. 80 supplementary Table I).

D. *Drosophila* larva force measurement

To show that our colored micropillar device can be used widely with organisms that show slithering and crawling motion, we measure, for the first time, the forces exerted by crawling *D. melanogaster* first instar larvae that are approximately 450–550 μm in diameter and 1300–1600 μm in length. The micropillar device used was identical to that used for *C. elegans*. The larva was transferred to the surface of the pillar device filled with PBS buffer using a brush where it proceeded to crawl on the pillar tips (schematic Figure 3(b1)).[43] This differs from how forces are measured in *C. elegans* where the organism sinusoidally undulates between the pillars on an agar surface (schematic Figure 3(a1)). The PDMS pillars that were not colored, were not visible even using different illumination angles (Figures 3(b2) and 3(b3)).[43] This drawback was completely eliminated when colored pillars were utilized (Figure 3(b4)).[43] We obtained very high contrast images of pillars at low light intensities using slanted illumination as shown in Figure 3(b4). This demonstrated the use of the device with a millimeter sized organism accompanied by a slight modification in experimental setup and no changes in the geometry of the device. The first instar was chosen so that entire body of the larva can be observed under the field of view of the microscope at our chosen magnification. Later stages with larger larval size such as second and third instar can, in principle, be studied using our device with a lower magnification lens.

The motion of ten larvae was imaged and recorded for approximately 45 s as they moved on top of the micropillars (supplementary Movie 2). The larva crawls by generating a peristaltic contraction wave that travels along the body that begins at its tail and ends at its head in forward crawling.[67,68] In backward crawling, the contraction wave travels from the head to the tail.

Majority of the time, the larvae crawl forward while backward crawling occurs less frequently and sometimes takes place as a response to aversive stimulus to the head of the larva.[67] Among the ten larvae tested, we found only one larva that crawled backward. No apparent reason for backward crawling could be observed on the device. We expect that lower moisture on part of the device could be a factor that promotes backward crawling. The peristaltic motion of the body was quantified by fitting an ellipse on the animal and recording the length of the major anterior-posterior axis along the larvae using the open source software ImageJ.[43,44] Due to the peristaltic wave, the measured length of the organism changes during locomotion reducing at the beginning of contraction cycle and increasing as the wave travels along the body. Force measurements with *Drosophila* on the device were carried out, wherein the pillars are imaged from the bottom such that projection of the full length of the pillar is visualized (Figure 3(b1)). Pillars under the larva were analyzed by fitting an ellipse around the pillar image. We observe that the pillar deflections along the central anterior-posterior axis of the larva correlate with the peristaltic waves that propagate along the length of the larva (Figure 5 (Multimedia view), Figures 8(b1) and 8(b2)).[43] The pillars near the central anterior-posterior axis along the body length were deflected the most compared to pillars near the periphery (see Ref. 80 for supplementary Figure 4). Therefore, the pillars closer to the anterior-posterior central axis of the larval body were selected to graph the correlation between the peristaltic contraction wave and the pillar deflections. The pillar that touched the posterior (tail) gets deflected before the pillar that touched the anterior (head) of the larvae (Figure 8(b1)). The opposite was seen for reverse crawling (Figure 8(b2)). The maximum force that a larva exerted on a single pillar was $5.84 \pm 1.03\,\mu$N (averaged over 10 larvae $\pm$ SD). The total average force applied by a single larva was $32.61 \pm 8.68\,\mu$N. The average force applied per pillar by a single larva was $1.58 \pm 0.39\,\mu$N that is about 1.5 times larger than the force applied by wild type young adult *C. elegans*.

The average wave frequency of 0.4 ± 0.2 Hz ($n = 10$) was calculated by counting the number of peristaltic waves over a period of 45 s for a larva moving on the pillars. The biomechanics of *Drosophila* larval crawling and the rhythmic peristaltic waves of the body wall muscles have been studied before.[67–71] Wave frequencies of $\sim$0.5 Hz for first instar larvae[71] and $\sim$1–1.5 Hz for third instar larvae have been reported previously.[67,70] It has been shown that sensory feedback is important in coordination of rhythmic muscle contractions in larval crawling.[67,70,72] The inhibition of sensory neurons in a larva moving on an agar surface has been shown to reduce the wave frequency from 1.5 Hz to less than 0.5 Hz.[67] A reduced crawling speed has also been reported for larvae moving on an agarose surface when the agarose concentration and thus stiffness of the surface was reduced.[73] *Drosophila* has been widely used as a genetic model organism to study the sensory feedback mechanism,[67,70,72] muscle functions,[74,75] aging related movement impairment,[76] etc. In our micropillar device, the diameter, spacing, and stiffness of the pillars may play an important role in mechanical stimulation of a larva. Such micropillar arrays can be used to quantify forces applied during different behaviours and can provide insight into the properties of mechanosensory feedback and kinematics of larval locomotion.

IV. CONCLUSIONS

We have developed a simple device that can be used to measure forces applied by two genetic model organisms with large differences in body sizes. Our micropillar array can assist in bringing genetic tools to understand factors that influence forces applied during locomotion. In this study, we developed a novel method of fabricating colored PDMS micropillars. The micropillar arrays fabricated using composite PDMS were calibrated using FemtoTools force sensors. There was a reduction in the elastic modulus due to the addition of dye to PDMS. We estimated the mechanical parameters of the dye-PDMS composite material using Yeoh hyperelastic model. This was essential for modeling the micropillars using FEA that we performed utilizing the Comsol Multiphysics^{TM} software. We observed that the measured micropillar stiffness was 20% larger than the stiffness calculated by the FEA model. This suggests that the micropillar stiffness should be calibrated directly using a force sensor instead of using the bulk material parameters for stiffness estimation. It is likely that the material parameters are not

preserved when one shifts from bulk material to a micrometer scale device. The ability to change the Young's modulus using different dye concentration also offers an ability to design pillars of varying stiffness. Such stiffness modifications can be used to access different ranges of force measurements from sub-micronewtons to a few 10s of micronewtons.

The advantage of colored micropillars is in their easy identification and tracking, which we have demonstrated using both *C. elegans* and *Drosophila* larvae. The algorithm used to track pillars can be readily adapted for different shapes and sizes of pillar and can be used for real time tracking as well. A semi-automated graphical user interface gave us the capability to analyze a large number of images quickly and with ease. Collapsing the forces measured over the large spatial and temporal range of a movie into a single value of average force applied per pillar offers a quick screening tool to compare various *C. elegans* strains.

All of the above advantages allowed us to rapidly analyze forces applied by multiple genotypes of *C. elegans*. The force measurement of *C. elegans* that has softer bodies and those that have disrupted sense of gentle mechanical touch suggested that the lower cuticle stiffness as well as the reduced ability to sense touch do not have significant effect on force generation during locomotion. The disruptions of body wall musculature however resulted in a significant reduction in the forces applied by the worm. It was also observed that the motility of the worms with mechanosensation defects, lower cuticle stiffness, and body wall muscle defects was reduced with worms that have defective body wall muscle having the largest degree. Thus, while reduced ability to apply forces affects the locomotion of the worm in the micropillar array, the reduced motility/locomotion may not indicate that the worm has reduced ability to apply forces on the micropillars.

We also demonstrate wider applicability of our simple device by recording forces generated by *D. melanogaster* larva during its locomotion. Our device successfully captured the peristaltic rhythm of the body wall muscles of the larva and allowed us to measure the forces applied on each deflected pillar during this motion. Our device offers a measurable range of force up to $\sim 8.4\,\mu$N in case of *C. elegans* that slither in between the pillars and $\sim 7\,\mu$N in case of *Drosophila* larvae that crawl on top of the pillars. Average maximum force of $4.4 \pm 1.24\,\mu$N for wild type *C. elegans* and $5.84 \pm 1.03\,\mu$N for *Drosophila* larvae was observed. Knowledge of such an average force range could be helpful in delivering a broad range of mechanical stimuli to an organism even without calculating forces applied on every pillar. Our device also offers the possibility of delivering a known mechanical stimulus consistently across the entire animal as opposed to the more typical single point acute stimulation. This distributed application of mechanical stimuli might be similar to some of the environments *C. elegans* and *Drosophila* larvae experience in their natural habitats.

The effect of the stiffness of mechanical environment of the organism on its locomotion could be examined using our micropillar arrays. Effects of such changes in environmental parameters have been reported earlier both for *C. elegans*[28,77–79] as well as *D. melanogaster* larvae.[73] Our device facilitates such studies where the modification of pillar stiffness can provide a large regime of mechanical richness in the environment. The initial rapid motion of *C. elegans* in our device suggests that our device can function as a tunable passive mechanical stimulator for genetic model organisms.

Our colored micropillar device is useful for force measurements on a wide range of animal sizes. The pillar device and the accompanying tracking software will help study several biological processes involving locomotion of crawling and slithering organisms. In addition our device offers a "self-stimulation" tool where the animals that do not have severe locomotory defects can move in a mechanically rich environment. This offers us a means to test the role of mechanical stimulation on locomotory biomechanics and on different *in vivo* cell biological processes.

ACKNOWLEDGMENTS

We thank CENSE, IISc, Spectroscopy/Analytical Test Facility, IISc and NCBS-TIFR Central Imaging Facility. We thank Professor Upendra Nongthomba, MRDG, IISc, India for providing

Drosophila larvae. We thank Koushika laboratory members for comments on the manuscript. We also thank Dr. Kaustubh Rau, Rishi Valley School, Dr. Namrata Gundiah, IISc, and Suchi Agrawal, IISc for critical comments on the manuscript. We also thank Sivakrishna Narra, IISc for helpful discussions and suggestions. Some strains were provided by the CGC, which is funded by NIH Office of Research Infrastructure Programs (P40 OD010440). Research funding was provided by HHMI-IECS Grant No. 55007425 to S.P.K.

[1]H. Takahashi, K. Matsumoto, and I. Shimoyama, in *Proceedings of IEEE International Conference on Micro Electro Mechanical Systems* (IEEE, 2013), Vol. 2, p. 59.
[2]L. Reinhardt and R. Blickhan, J. Exp. Biol. **217**, 704 (2014).
[3]Y. Shen, U. C. Wejinya, N. Xi, and C. A. Pomeroy, Proc. Inst. Mech. Eng., Part H **221**, 99 (2007).
[4]S.-J. Park, M. B. Goodman, and B. L. Pruitt, Proc. Natl. Acad. Sci. U. S. A. **104**, 17376 (2007).
[5]N. Zumstein, O. Forman, U. Nongthomba, J. C. Sparrow, and C. J. H. Elliott, J. Exp. Biol. **207**, 3515 (2004).
[6]J. C. Doll, N. Harjee, N. Klejwa, R. Kwon, S. M. Coulthard, B. Petzold, M. B. Goodman, and B. L. Pruitt, Lab Chip **9**, 1449 (2009).
[7]A. Ghanbari, V. Nock, S. Johari, R. Blaikie, X. Chen, and W. Wang, J. Micromech. Microeng. **22**, 095009 (2012).
[8]M. Dembo and Y. L. Wang, Biophys. J. **76**, 2307 (1999).
[9]C. M. Lo, H. B. Wang, M. Dembo, and Y. L. Wang, Biophys. J. **79**, 144 (2000).
[10]S. S. Ng, C. Li, and V. Chan, Interface Focus **1**, 777 (2011).
[11]C. R. Nuttelman, D. J. Mortisen, S. M. Henry, and K. S. Anseth, J. Biomed. Mater. Res. **57**, 217 (2001).
[12]D. T. Tambe, C. C. Hardin, T. E. Angelini, K. Rajendran, C. Y. Park, X. Serra-Picamal, E. H. Zhou, M. H. Zaman, J. P. Butler, D. A. Weitz, J. J. Fredberg, and X. Trepat, Nat. Mater. **10**, 469 (2011).
[13]J. L. Tan, J. Tien, D. M. Pirone, D. S. Gray, K. Bhadriraju, and C. S. Chen, Proc. Natl. Acad. Sci. U. S. A. **100**, 1484 (2003).
[14]U. Dammer, O. Popescu, P. Wagner, D. Anselmetti, H. J. Güntherodt, and G. N. Misevic, Science **267**, 1173 (1995).
[15]T. G. Kuznetsova, M. N. Starodubtseva, N. I. Yegorenkov, S. A. Chizhik, and R. I. Zhdanov, Micron **38**, 824 (2007).
[16]H. H. Fang, K. Y. Chan, and L. C. Xu, J. Microbiol. Methods **40**, 89 (2000).
[17]K. D. Webster, A. Crow, and D. A. Fletcher, PLoS One **6**, e17807 (2011).
[18]S. Yang and T. Saif, Rev. Sci. Instrum. **76**, 044301 (2005).
[19]C. G. Galbraith and M. P. Sheetz, Proc. Natl. Acad. Sci. U. S. A. **94**, 9114 (1997).
[20]A. Folch and M. Toner, Biotechnol. Progr. **14**, 388 (1998).
[21]S. L. Peterson, A. McDonald, P. L. Gourley, and D. Y. Sasaki, J. Biomed. Mater. Res. Part A. **72A**, 10 (2005).
[22]Z. Yue, X. Liu, P. J. Molino, and G. G. Wallace, Biomaterials **32**, 4714 (2011).
[23]F. Schneider, T. Fellner, J. Wilde, and U. Wallrabe, J. Micromech. Microeng. **18**, 065008 (2008).
[24]R. N. Palchesko, L. Zhang, Y. Sun, and A. W. Feinberg, PLoS One **7**, e51499 (2012).
[25]A. L. Larsen, K. Hansen, P. Sommer-Larsen, O. Hassager, A. Bach, S. Ndoni, and M. Jørgensen, Macromolecules **36**, 10063 (2003).
[26]I. K. Lin, Y. M. Liao, Y. Liu, K. S. Ou, K. S. Chen, and X. Zhang, Appl. Phys. Lett. **93**, 251907 (2008).
[27]K. Kim, R. Taylor, J. Y. Sim, S.-J. Park, J. Norman, G. Fajardo, D. Bernstein, and B. L. Pruitt, Micro Nano Lett. **6**, 317 (2011).
[28]S. Johari, V. Nock, M. M. Alkaisi, and W. Wang, Lab Chip **13**, 1699 (2013).
[29]A. Llobera, S. Demming, H. N. Joensson, J. Vila-Planas, H. Andersson-Svahn, and S. Büttgenbach, Lab Chip **10**, 1987 (2010).
[30]M. A. Cartas-Ayala and S. Bose, RSC Chips and Tips, November 2011.
[31]I. D. Johnston, D. K. McCluskey, C. K. L. Tan, and M. C. Tracey, J. Micromech. Microeng. **24**, 035017 (2014).
[32]A. P. Gerratt, I. Penskiy, and S. Bergbreiter, J. Micromech. Microeng. **23**, 045003 (2013).
[33]F. Gaudière, I. Masson, S. Morin-Grognet, O. Thoumire, J.-P. Vannier, H. Atmani, G. Ladam, and B. Labat, Soft Matter **8**, 8327 (2012).
[34]O. H. Yeoh, Rubber Chem. Technol. **66**, 754 (1993).
[35]L. Ci, J. Suhr, V. Pushparaj, X. Zhang, and P. M. Ajayan, Nano Lett. **8**, 2762 (2008).
[36]Q. Cheng, Z. Sun, G. A. Meininger, and M. Almasri, Rev. Sci. Instrum. **81**, 106104 (2010).
[37]S. Brenner, Genetics **77**, 71 (1974), PDF available at http://www.genetics.org/content/77/1/71.full.pdf+html.
[38]H. F. Epstein, R. H. Waterston, and S. Brenner, J. Mol. Biol. **90**, 291 (1974).
[39]A. R. MacLeod, R. H. Waterston, R. M. Fishpool, and S. Brenner, J. Mol. Biol. **114**, 133 (1977).
[40]J. M. Zengel and H. F. Epstein, Proc. Natl. Acad. Sci. U. S. A. **77**, 852 (1980).
[41]C. Savage, M. Hamelin, J. G. Culotti, A. Coulson, D. G. Albertson, and M. Chalfie, Genes Dev. **3**, 870 (1989).
[42]M. Chalfie and J. Sulston, Dev. Biol. **82**, 358 (1981).
[43]S. M. Khare, V. Venkataraman, and S. P. Koushika, in 18th International Conference on Miniaturized Systems for Chemistry and Life Science (The Chemical and Biological Microsystems Society, 2014).
[44]W. S. Rasband, ImageJ, U.S. National Institute of Health, Bethesda, Maryland, 1997–2014, see http//imagej.nih.gov/ij/.
[45]J. Zhang, H. Chen, J. Sheng, L. Liu, Y. Wang, and S. Jia, Theor. Appl. Mech. Lett. **3**, 054011 (2013).
[46]B. Mosadegh, P. Polygerinos, C. Keplinger, S. Wennstedt, R. F. Shepherd, U. Gupta, J. Shim, K. Bertoldi, C. J. Walsh, and G. M. Whitesides, Adv. Funct. Mater. **24**, 2163 (2014).
[47]T. V. Korochkina, E. H. Jewell, T. C. Claypole, and D. T. Gethin, Polym. Test. **27**, 778 (2008).
[48]M. Wissler and E. Mazza, Sens. Actuators, A **120**, 184 (2005).
[49]A. M. Bueche, J. Polym. Sci. **25**, 139 (1957).
[50]A. Lion, Continuum. Mech. Thermodyn. **8**, 153 (1996).
[51]A. Saleem, L. Frormann, and A. Soever, Polymers **2**, 200 (2010).
[52]D. R. Paul and J. E. Mark, Prog. Polym. Sci. **35**, 893 (2010).

[53]S. R. Gaboury and M. W. Urban, Polymer **33**, 5085 (1992).
[54]N. Stafie, D. F. Stamatialis, and M. Wessling, Sep. Purif. Technol. **45**, 220 (2005).
[55]C. Thacker, J. A. Sheps, and A. M. Rose, Cell. Mol. Life Sci. **63**, 1193 (2006).
[56]T. L. Gumienny, L. T. MacNeil, H. Wang, M. de Bono, J. L. Wrana, and R. W. Padgett, Curr. Biol. **17**, 159 (2007).
[57]B. C. Petzold, S.-J. Park, E. A. Mazzochette, M. B. Goodman, and B. L. Pruitt, Integr. Biol. **5**, 853 (2013).
[58]N. J. Dibb, D. M. Brown, J. Karn, D. G. Moerman, S. L. Bolten, and R. H. Waterston, J. Mol. Biol. **183**, 543 (1985).
[59]T. M. Rogalski, E. J. Gilchrist, G. P. Mullen, and D. G. Moerman, Genetics **139**, 159 (1995); available online at http://www.genetics.org/content/139/1/159.abstract?sid=8f3b766a-260f-47c1-bb87-9f0344e7ea74#cited-by.
[60]R. O'Hagan, M. Chalfie, and M. B. Goodman, Nat. Neurosci. **8**, 43 (2005).
[61]A. Bounoutas, R. O'Hagan, and M. Chalfie, Curr. Biol. **19**, 1362 (2009).
[62]B. C. Petzold, S. J. Park, P. Ponce, C. Roozeboom, C. Powell, M. B. Goodman, and B. L. Pruitt, Biophys. J. **100**, 1977 (2011).
[63]S. Park, H. Hwang, S. W. Nam, F. Martinez, R. H. Austin, and W. S. Ryu, PLoS One **3**, e2550 (2008).
[64]A. Albeg, C. J. Smith, M. Chatzigeorgiou, D. G. Feitelson, D. H. Hall, W. R. Schafer, D. M. Miller, and M. Treinin, Mol. Cell. Neurosci. **46**, 308 (2011).
[65]E. Cohen, E. Yemini, W. Schafer, D. G. Feitelson, and M. Treinin, J. Exp. Biol. **215**, 3639 (2012).
[66]J. Korta, D. A. Clark, C. V. Gabel, L. Mahadevan, and A. D. T. Samuel, J. Exp. Biol. **210**, 2383 (2007).
[67]C. L. Hughes and J. B. Thomas, Mol. Cell. Neurosci. **35**, 383 (2007).
[68]J. Gjorgjieva, J. Berni, J. F. Evers, and S. J. Eglen, Front. Comput. Neurosci. **7**, 24 (2013).
[69]N. Scantlebury, R. Sajic, and A. R. Campos, Behav. Genet. **37**, 513 (2007).
[70]W. Song, M. Onishi, L. Y. Jan, and Y. N. Jan, Proc. Natl. Acad. Sci. U. S. A. **104**, 5199 (2007).
[71]E. S. Heckscher, S. R. Lockery, and C. Q. Doe, J. Neurosci. **32**, 12460 (2012).
[72]J. C. Caldwell, M. M. Miller, S. Wing, D. R. Soll, and D. F. Eberl, Proc. Natl. Acad. Sci. U. S. A. **100**, 16053 (2003).
[73]A. A. Apostolopoulou, F. Hersperger, L. Mazija, A. Widmann, A. Wüst, and A. S. Thum, Front. Behav. Neurosci. **8**, 11 (2014).
[74]G. Kaushik, A. C. Zambon, A. Fuhrmann, S. I. Bernstein, R. Bodmer, A. J. Engler, and A. Cammarato, J. Cell. Mol. Med. **16**, 1656 (2012).
[75]D. M. Swank, Methods **56**, 69 (2012).
[76]M. A. Jones and M. Grotewiel, Exp. Gerontol. **46**, 320 (2011).
[77]S. R. Lockery, K. J. Lawton, J. C. Doll, S. Faumont, S. M. Coulthard, T. R. Thiele, N. Chronis, K. E. McCormick, M. B. Goodman, and B. L. Pruitt, J. Neurophysiol. **99**, 3136 (2008).
[78]S. Pandey, Adv. Biosci. Biotechnol. **02**, 409 (2011).
[79]A. Parashar, R. Lycke, J. A. Carr, and S. Pandey, Biomicrofluidics **5**, 024112 (2011).
[80]See supplementary material at http://dx.doi.org/10.1063/1.4906905 for screen shots of pillar tracking software, additional histograms of region-wise forces for different stains and body regions, number of pillars touched during motion, and derivation of the small deformation shear modulus equation.